Archaeological Prospection
Archaeol. Prospect. **17**, 49–60 (2010)
Published online 28 December 2009 in Wiley InterScience
(www.interscience.wiley.com) DOI: 10.1002/arp.371

Decorrugation, Edge Detection, and Modelling of Total Field Magnetic Observations from a Historic Town Site, Yellowstone National Park, USA

STEVEN D. SHERIFF[1]*, DOUGLAS MACDONALD[2] AND DAVID DICK[2]

[1] *Department of Geosciences, University of Montana, Missoula, Montana, USA*
[2] *Department of Anthropology, University of Montana, Missoula, Montana, USA*

ABSTRACT Cinnabar, Montana is a historic town site and railroad depot near the northern edge of Yellowstone National Park and was inhabited between 1883 and 1903. Remains of foundations and old photographs help determine the area of the town, but the south and east limits are unknown. We acquired total field magnetic intensity data to help determine the full extent of the town. Randomly distributed ferrous magnetic sources on the surface and typical noise associated with acquisition complicate the signal. To separate signal and noise we applied filtering and edge detection techniques common in the aeromagnetic industry to our data. Regional removal, decorrugation, upward continuation, and edge detection successfully separated signal and noise. Following filtering, we extracted two larger anomalies from the data set. For those two anomalies, we estimated the edges of their causative sources by calculating the maxima in the horizontal gradient of their anomalies and by inverse modelling those sources; both methods yield similar results. An archaeological test unit excavation within one of the anomalies clearly indicates the remains of buried domestic features, the foundation to a house or other building associated with the late nineteenth to early twentieth century use of Cinnabar. Thus the southeast extent of Cinnabar is greater than previously thought. The lack of surface indicators or adequate historic photography precluded the identification of this buried feature without the aid of the magnetic study. Copyright © 2009 John Wiley & Sons, Ltd.

Key words: Decorrugation; edge detection; filtering; magnetic; archaeology

Introduction

The Montana–Yellowstone Archaeological Project, a joint endeavour of The University of Montana Department of Anthropology and Yellowstone National Park, studies the prehistory and history of the northern portion of Yellowstone National Park (MacDonald, 2007). The historical component of interest entails identifying the former location and extent of Cinnabar (Figure 1), the original Northern Pacific Railroad depot for visitors to Yellowstone National Park between 1883 and 1903. The main area of Cinnabar contains the remains of 11 building foundations, identifiable as depressions upon the current ground surface. Yet a modern layer of up to 10 cm of silty aeolian sand complicates recognition of the vestiges of old structures in much of the area.

Individuals travelling to Yellowstone on the railroad photographed the central areas of Cinnabar during the late nineteenth century. Limited oral history along with two old photographs provides some guidance to the limits of Cinnabar. The historic photographs also helped corroborate archaeological field efforts within specific building foundations, such as the hotel, store, privy, and blacksmith shop. The area southeast of central Cinnabar (Figure 2) lacks building foundations, any adequate photography, or any surface-indication of former buildings. However, the area contains a scatter of historical debris, a possible indicator of buried archaeological deposits associated with Cinnabar.

Our experience, supported by this study and others (e.g. Kvamme, 1998; Larson *et al.*, 1999), is that

* Correspondence to: S. D. Sheriff, Department of Geosciences, University of Montana, Missoula, Montana, USA.
E-mail: steven.sheriff@umontana.edu

Received 8 December 2008
Revised 18 April 2009
Accepted 11 November 2009

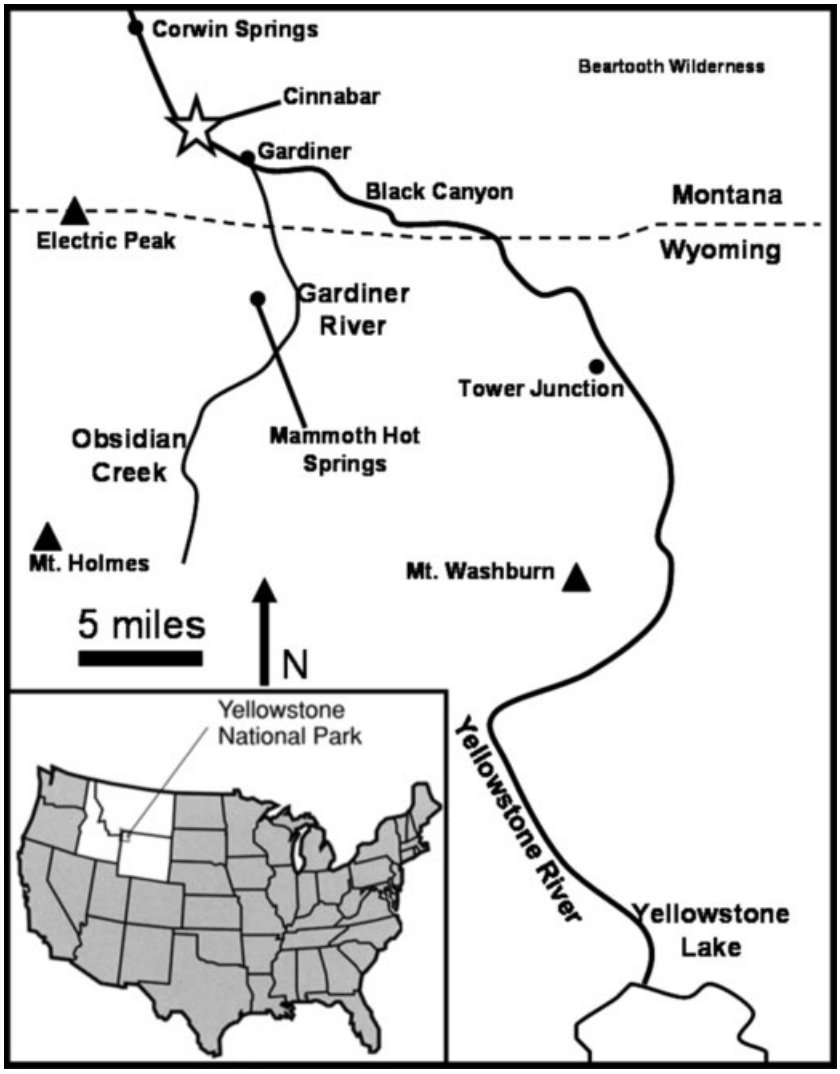

Figure 1. Index map locating the historic town of Cinnabar near Yellowstone National Park, Montana, USA.

randomly scattered ferromagnetic debris complicates magnetic surveys and interpretation at historic town sites, particular mining towns, in the western USA. In particular, measuring the gradient of the magnetic field, rather than the total field, often results in isolating debris laying on or near the surface (where visual detection is more efficient) and obscuring the signal from larger buried features. Tabbagh (2003) also notes that with appropriate filtering total field observations can be archaeologically advantageous to measuring the vertical gradient of the magnetic field. Thus, to assess the town boundaries and the viability of magnetic surveying in the area, we acquired total field magnetic data over about 0.56 ha at the southeast edge of the town site away from visible foundations. We then successfully processed those data utilizing techniques standard in aeromagnetic and ground magnetic exploration for mineral and energy resources using readily available software. Though not commonly used in archaeological applications, we exploit these methods not only for experimentation but because they offer a number of advantages for filtering noisy data, separating sources, edge detection, and preparation for existing visualization and inversion packages (e.g. MAG3D, 2007). Test unit excavations following the magnetic survey clearly indicate the remains of a buried domestic feature, perhaps the foundation to a house or other building, associated with the late nineteenth to early twentieth century use of Cinnabar. Thus, application

DOI: 10.1002/arp

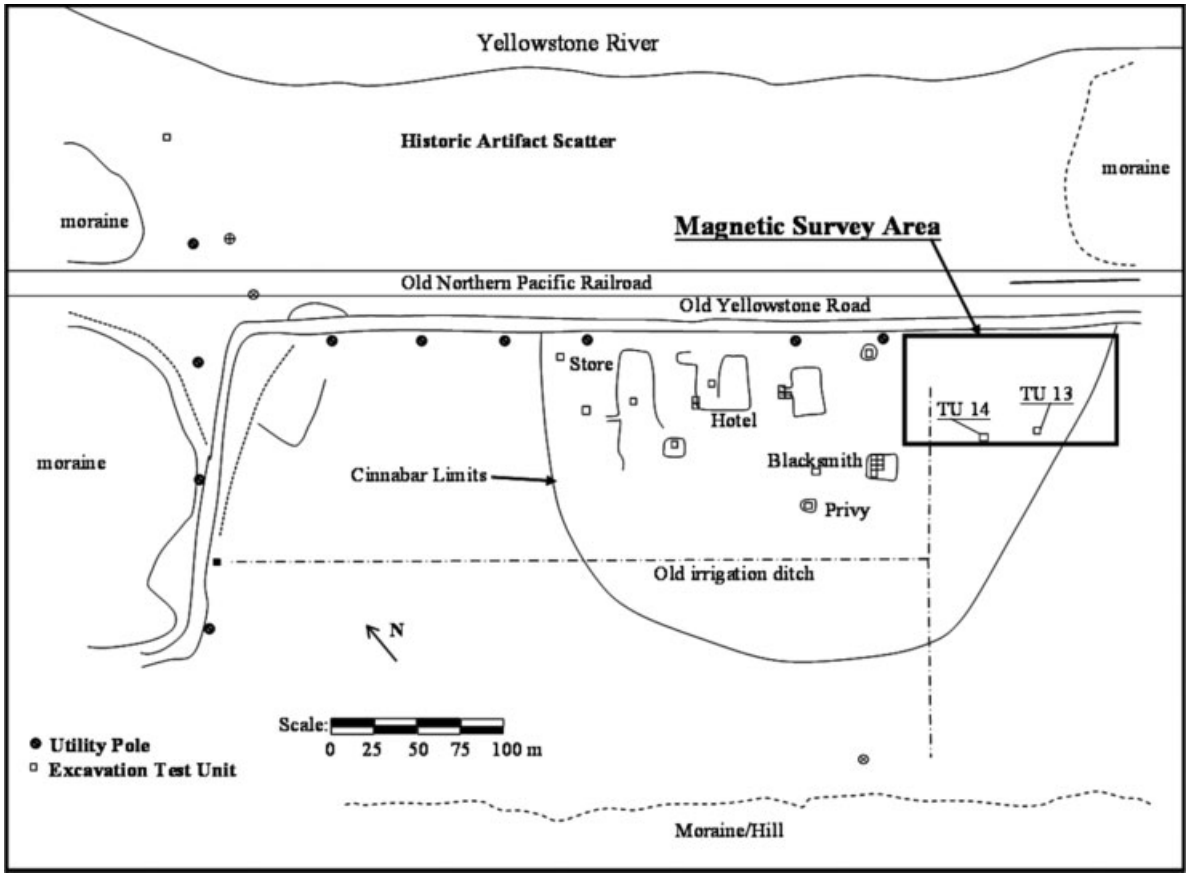

Figure 2. Site plan map for the archaeological study at Cinnabar.

of these processing techniques in areas of archaeological interest with difficult acquisition situations or substantial surface scatter is worthwhile.

Magnetic survey

Initially we planned on integral GPS guidance during the acquisition of our total field magnetic intensity observations. Unfortunately, antenna failure lead to guiding transects with ropes and a tape measure. Either method of guidance includes an error component though that from RTK GPS guidance is much smaller in amplitude than that for walking (e.g. Gaffney *et al*., 2008). Walking marked lines typically adds noise to the desired signal due to mislocations, variable walking speeds, and directionally dependent sampling frequencies; rugged surface conditions add additional noise during acquisition. Randomly distributed ferrous magnetic sources distributed throughout the reconnaissance area introduce additional point-source noise to our data. Our experience is that similar easily visible random magnetic sources on the ground surface commonly contaminate magnetic signals at historic town sites particularly those associated with mining. Those sources on the surface dominate observations of the magnetic gradient and subtle signals from deeper causative sources are much more difficult to retrieve from gradiometry data. Thus, we chose total field observations over gradiometry so that we could later filter the effects of the scattered surface debris and isolate signal from foundations and living surfaces of the former town site. For filtering, we experimented with several filtering techniques developed for aeromagnetic scale surveys designed to delineate tectonic features or for exploration by the energy and mining industries. These techniques proved their usefulness and considerably enhanced our interpretation of the data.

We acquired total field magnetic intensity observations (Figure 3) at 5 Hz while walking bidirectional transects spaced 1 m apart using a Geometrics G858 caesium vapour magnetometer. We collected our total magnetic field intensity data in about three hours on a

DOI: 10.1002/arp

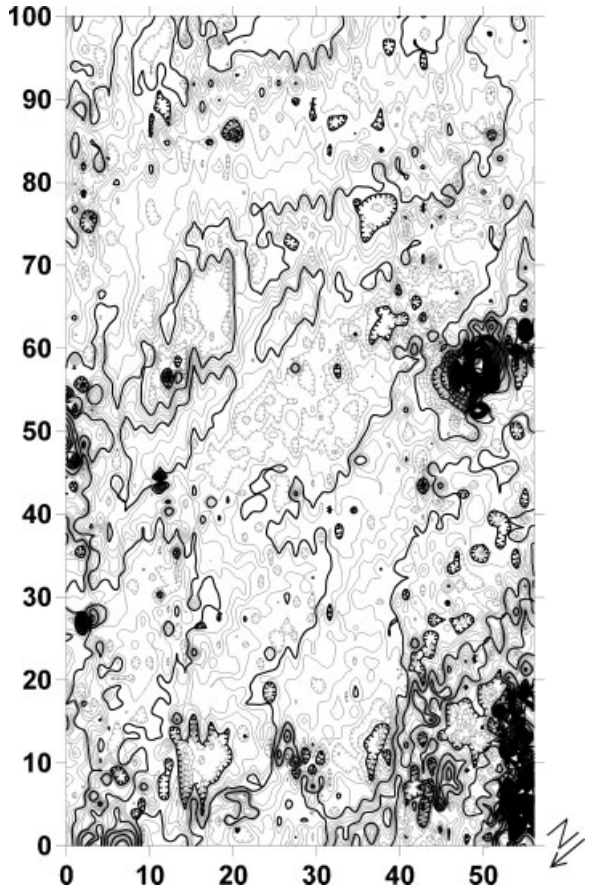

Figure 3. Total field intensity contoured at 5 nanotesla (nT) with a range of 2123 nT; horizontal dimensions are metres. The vertical axis trends 130° east of north. The bidirectional acquisition direction, with 1 m spacing, is vertical in the figure.

magnetically quiet day as observed by NOAA (NOAA, 2009) and our on-site observations. Successive and repeat observations at stationary sites during the day showed minimal high-frequency variance of the total magnetic field. Regardless, given our lack of a recording base station, geomagnetic variations will be present in the data. The frequency spectrum of such geomagnetic variance can be broad. Low-frequency components have periods similar to the acquisition time of several transects and longer. High-frequency components have periods ranging from the time for acquiring a few observations to that for acquiring a few transects. In the filtering described below, we deal with the possibility of long period geomagnetic variation in combination with that for regional, or geological, sources. We treat the potential effects of high-frequency variance with filtering techniques adapted from the energy and mining industry. This proved successful as is demonstrated by the final maps. The ultimate anomalies of interest in this project have amplitudes of 10s to 100s of nanoteslas.

Our total magnetic field intensity observations (Figure 3), gridded by kriging, include features at several scales. First, there is corrugation (also referred to as striping, zigzag, herringbone, or staggering) which is typical in ground and airborne magnetic surveys where observations are acquired at relatively high spatial frequency along more widely spaced transects. Despite the usual efforts to keep the sensor a constant distance from the ground, bunch grass, rough surfaces, rocks and wind combine to interfere with the operator and impact the distance of the sensor from the ground while walking and acquiring observations at 5 Hz. This manifests as linear magnetic anomalies highly correlated with the direction of acquisition. There are several methods for decorrugating magnetic data.

Urquhart (1988) developed a widely used technique for decorrugation filtering of aeromagnetic data. We use this, as discussed below, because it operates rapidly on a grid of data, allows visual inspection of results from successively larger filter operators, and thus empirical determination of a suitable operator size. Urquhart's (1988) method is also readily available in public domain software (Phillips, 1997, 2007). Other methods are more common among archaeological geophysicists who have generally performed line by line adjustments as opposed to filtering a complete grid of data. For example Ciminale and Loddo (2001) align nearest neighbour traces using correlation, Becker (2001) uses a GPS-based speed dependent correction, and Odah *et al*. (2005) translate every other line by up to 1.5 m to clean their data. Those choices have been in part dependent on available equipment and accompanying software. More recent contributions from Tsivouraki and Tsokas (2007) and Fedi and Florio (2003) address denoising and corrugation respectively and provide alternative methods for grid filtering based on the discrete wavelet transform. Regardless of the algorithm, decorrugating a magnetic map yields a better estimate of anomalies due to other causative sources of greater interest.

Second, numerous small features on the map at the scale of 0.5 to 2 m result from randomly scattered ferrous sources on the ground surface. At the Cinnabar site, these objects include horseshoes, bits of cast iron stoves, scrap sheet metal, nails, and the like. Such objects have a combination of induced and remanent magnetizations. An induced magnetization would typically cause a dipolar signature which is a paired set of high and low amplitudes with the low-amplitude offset towards magnetic north (12.5° east

DOI: 10.1002/arp

at the study location). If there is a remanent magnetization vector added to the induced magnetization, the dipole signature points in the direction of the resultant vector.

Third, two high-amplitude anomalies at the centre and lower right-hand edge (Figure 3) dominate the contour scale and swamp any subsequent colour contour spectra presentations of the complete area. The lower right anomaly ($x = 55$, $y = 5$) had sufficient ground disturbance and artefacts to warrant nearby test excavations before the magnetic survey. The central-right anomaly ($x = 50$, $y = 60$) presented no observable evidence at the surface. We discuss both these anomalies below. Removing their impact from the total field magnetic intensity map highlights the magnetic signature of some natural features on the map and allows independent interpretation and modelling of the high-amplitude anomalies.

Finally, there are some longer wavelength (10 m east–west) signals which trend north–south through the area. These features correlate with subtle drainages, apparent on satellite imagery, that appear to be diverted around the area of investigation. Thus the anomalies may result from variable concentration of magnetic minerals in old fluvial deposits. Yet, in the final analysis, there is some suggestion that a few may be cultural features.

Regional removal, decorrugation, and upward continuation

The ambient geomagnetic field strength, about 54 000 nT in our area, dominates the scalar value of total magnetic field intensity and is very consistent across most surveys of archaeological scale. Typically one removes the regional component by a scalar subtraction of the mean value of the acquired observations or by fitting and subsequently subtracting a low-order polynomial surface fit to the data. We removed the regional field from our data by subtracting a least squares best-fit plane that decreases about $0.8\,\mathrm{nT\,m^{-1}}$ to the northeast.

Decorrugating by Urquhart's (1988) method involves three general steps. The first step uses a low-pass frequency filter to separate the grid of data into its short- and long-wavelength components in the acquisition direction. Next, the resulting long-wavelength component of the grid is long-wavelength filtered (again with a low-pass frequency filter) in the direction perpendicular to the acquisition direction. It is this direction, perpendicular to acquisition, which contains short wavelength components resulting from variable heights and nonlinear positioning of the sensor during acquisition of the magnetic observations. The low-pass filter removes the short wavelength components perpendicular to the acquisition direction; these short-wavelength components result in corrugations observed in the contoured data. This second step yields a smooth long-wavelength grid. Finally, add the smooth long-wavelength grid to the short-wavelength components isolated in the first step. The result is decorrugated (Figure 4). We used Phillips (1997, 2007) implementations for decorrugating and much of the subsequent filtering.

Iterative experimentation is necessary when separating the grids into short- and long-wavelength components for decorrugation. The best choice of filter wavelengths is determined by examining successive filtering experiments with increasing wavelengths. If one chooses a long-wavelength filter that is too long, then images of the noise will contain too much archaeological or geological information. Examining the decorrugated results allows visual confir-

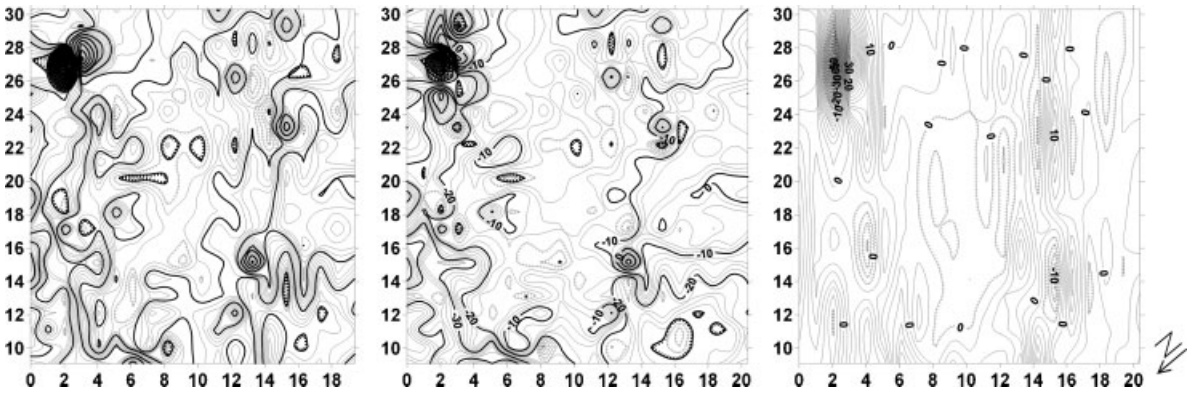

Figure 4. The left-hand image is representative of the total magnetic intensity map with data acquisition parallel to the vertical axis. The central image has had the regional removed and is decorrugated. The right-hand image is the corrugation removed from the left-hand image to produce the central image. Each map is contoured at 2 nT. The ranges, left to right in nT, for the maps are 258 nT, 169 nT and 94 nT respectively.

DOI: 10.1002/arp

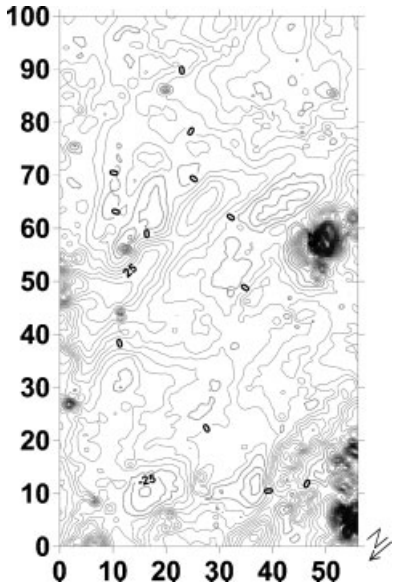

Figure 5. Field intensity contoured at 5 nT following regional removal, decorrugation and upward continuation of 0.5 m; total range is 653 nT.

mation that you are removing the correct wavelengths. Ultimately, this is subjective image processing and the greater the spectral overlap of signal and noise, the more difficult the decision. We used filter lengths of nine samples and nine lines along and across acquisition lines respectively. Representative subgrids from our total magnetic intensity grid show the positive effects of regional removal and decorrugation along with an example of the aliasing parallel to the acquisition direction that we removed (Figure 4).

Following decorrugation, we further attenuated high-frequency noise by upward continuing the data (Figure 5) by 0.5 m (one half of our line spacing during acquisition) using standard Fast Fourier Transform (FFT) techniques for level-to-level continuation (e.g. Blakely, 1995). Before calculating the forward FFT for this and subsequent filtering steps we extended the grid by 20% and cosine tapered the result to reduce edge effects and aliasing (Phillips, 1997). Upward continuation mathematically transforms the data measured on one surface to the magnetic field values that would be measured on another surface farther from causative sources. The shorter the wavelength (higher spatial frequency) of the upward continued anomaly, the greater the attenuation. Typically, upward continuation by an amount equal to or less than line spacing attenuates short wavelength noise due to variable motion of the sensor and sources on the surface without undue loss of signal from more significant causative sources. Upward continuation by half of our line spacing produced distinct, characteristic anomalies (Figure 6). These anomalies (Figure 6) as enhanced by regional removal, decorrugation, and upward continuation are similar to our expectations for anomalies caused by deeper sources such as foundations with spatial dimensions of several metres. That is, the overall anomalies are similar in scale to a building's footprint (e.g. Larson *et al*., 1999) while magnetic anomalies from individual foundation walls broaden as the depth to their tops increases. We now focus on those anomalies because they are of the appropriate spatial scale of interest for our investigation.

Edge detection on isolated anomalies

On inspection of our processed data, we isolated two higher amplitude anomalies (Figure 6) with length scales greater than 4 m that dominate the contour scale

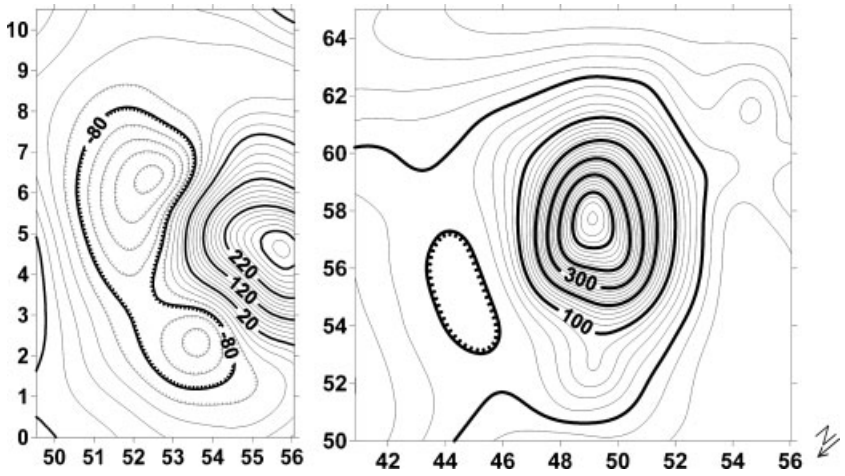

Figure 6. Two anomalies isolated for further interpretation. Each is decorrugated and upward continued by 0.5 m. Contour interval is 20 nT.

DOI: 10.1002/arp

of our total field intensity data. Each anomaly is within our scale of interest for discovering and delineating structures at the periphery of the Cinnabar site. One was the site of preliminary excavation before the magnetic survey and the second showed no readily discernible ground evidence of a historic structure and is beyond the area where a historic photograph showed the limits of the town. We extracted the two high-amplitude anomalies from the total data set after removing the ambient field, decorrugating, and upward continuing as discussed above.

Given good residual magnetic maps, isolating a target anomaly is a straightforward procedure. For features the size of foundations or compacted living surfaces applying edge detection techniques to the resulting anomalies helps guide the location of initial excavations. A number of edge detection techniques beyond traditional maps of first and second vertical derivatives exist (e.g. Blakely and Simpson, 1986; Roest *et al*., 1992; Thurston and Smith, 1997; Fedi and Florio, 2001; Cooper and Cowan, 2008) and several are implemented by Phillips (1997, 2007). As one would expect, the more that such methods depend on higher order derivatives the more susceptible they are to noise in the data set. Despite decorrugation and upward continuation of the data set, our observations from a historic town site with significant debris on the surface still contain short wavelength anomalies associated with that debris. Thus to delineate edges on the isolated anomalies (Figure 6) we use the horizontal gradient method (HGM) of Blakely and Simpson (1986), which only requires first-order derivatives. The value calculated in HGM analysis is the square root of the sum of the squared derivatives of the field in the x and y coordinate directions.

The horizontal gradient method requires that one first subject the magnetic data to one of two different but related transformations. Reduction to pole (RTP) is an FFT-based transformation (e.g., Blakely, 1995) that yields a phase-shifted anomaly as if the causative source is located at the magnetic pole, thereby removing most of the dipolar character of the signal. Poisson's relation shows that for a body with both uniform magnetic susceptibility and density the magnetic potential is proportional to the derivative of the gravity potential in the direction of magnetization. Baranov (1957) exploited this relation to develop the pseudogravity transformation, another linear filter typically applied in the Fourier domain. The pseudogravity transformation yields magnetic scalar potential with vertical magnetization, hence 'pseudogravity' in that the transformed field looks more like a gravity anomaly, centred over the source, which was among Baranov's (1957) intentions. The pseudogravity transformation also accentuates long wavelengths while attenuating shorter wavelengths. Reduction to pole and pseudogravity are related in that the pseudogravity is the first vertical integral of the reduction to pole transform (e.g. Phillips *et al*., 2007). The dependence on RTP transformation presents problems in areas of low latitude with shallow magnetic inclination, which is not the case at Yellowstone National Park. For our transformations, we assumed induced magnetization of the soil and sediment was much greater than any remanent magnetization and used the local declination and inclination of 12.5° east, 70° down, respectively.

Typical applications for which HGM was developed have depth scales of kilometres. In that situation, the determination of the appropriate transformation (RTP or pseudogravity) drives the ability to obtain depth estimates from the method depending on whether the expected source consists of thin or thick sheets. When used solely for edge detection, HGM on a pseudogravity transformation tends to have fewer false contacts than when calculated for an RTP transformation that includes more high frequency effects due to the vertical integral relation of pseudogravity to RTP. In practice, comparing HGM on the two transformations allows one to see where they overlap.

The top two quartiles of maxima in the horizontal gradient of the pseudogravity superposed on the two extracted anomalies outline the estimates of the edges of subsurface causative sources (Figure 7) creating the magnetic anomalies. Thus, the maxima serve to help locate initial excavation units. Maxima shown with larger symbols are more significant. The lower two quartiles of maxima (not shown) highlight lesser gradients in the anomalies we judge to be less significant for our interests. These may be from deeper natural sources, remaining noise, or artefacts in the data. For these anomalies, maxima of the horizontal gradient of reduction to pole and pseudogravity transformations were essentially equivalent.

Modelling and depth estimates

Magnetic data contain no inherent depth information. Yet, steep gradients on anomalies typically indicate shallow sources and help constrain modelling results, which yield a three-dimensional model of the subsurface. Another approach to depth estimation uses equivalent sources. Jacobsen (1987) made a strong case for using upward continuation filtering as a method for separating causative sources from various

DOI: 10.1002/arp

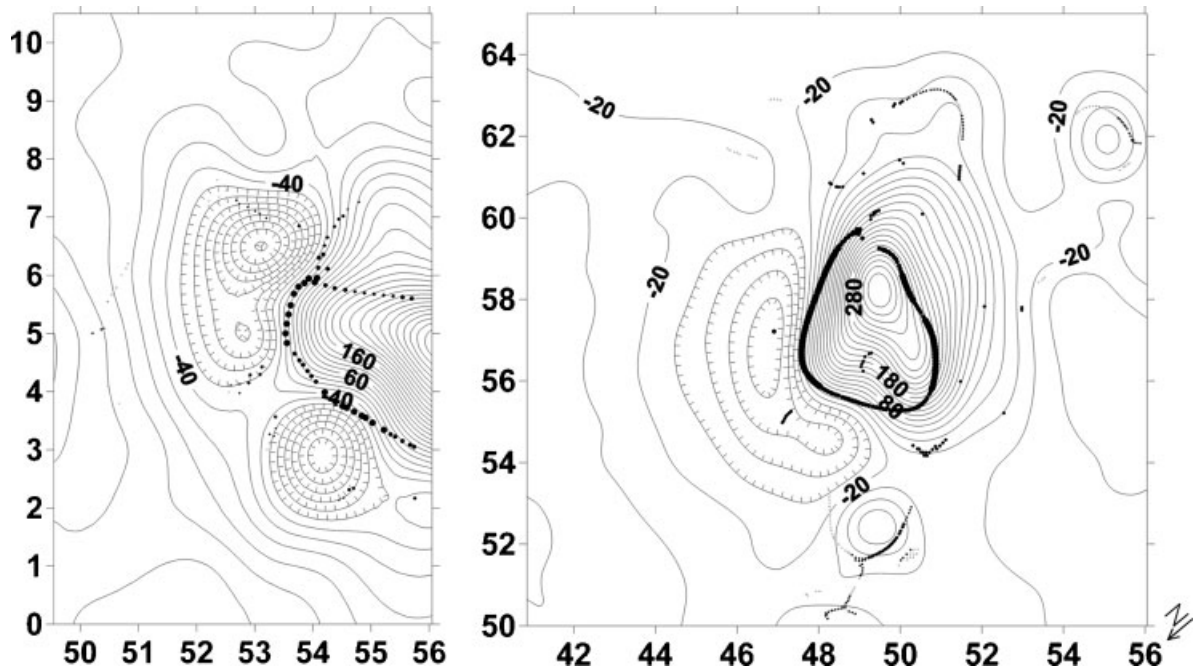

Figure 7. Total field intensity of isolated anomalies contoured at 20 nT. Dots are the superposed maxima of the horizontal gradient of the pseudogravity. Darker and larger dots represent more significant maxima and locate subsurface edges of the causative sources.

depths. Thus, we experimented with two different approaches to estimating the depth or bottom of the subsurface sources causing the anomalies (Figure 7).

First, we inverted the total field data (Li and Oldenburg, 1996; MAG3D, 2007). Those inversions result in best-fit models of subsurface magnetic susceptibility that produce their observed anomalies closely. These three-dimensional models thereby provide estimates of depth as well as edges. The plan view (Figure 8) and three-dimensional subsurface models (Figure 9) generated by MAG3D (2007) compare very well with the maxima of the horizontal gradient of the field intensity results. Thus the two independent methods yield very similar estimates for the edges of the causative sources. The subsurface magnetic susceptibility models (Figure 9) from MAG3D (2007) are three dimensional and thus estimate the depth extent of the sources as well.

We experimented with MAG3D (2007) inversions by generating and constraining solutions a number of different ways, a typical procedure to verify robustness of inverse solutions. For every case, for both anomalies, the depth to the bottom of the causative source was always within about 2 m or less of the ground surface. Piro et al. (2007) also successfully used MAG3D (2007) for an archaeological investigation and provide further insights and analysis for its application to other situations. Estimating the depth of sources by differencing successive upward continuations (Jacobsen, 1987) for both of the anomalies suggests that greater than 90% of the equivalent sources are shallower than 2 m. Thus, either method indicates sources within the depth range we expect for foundations and further suggest that deeper geological sources do not generate the anomalies.

Field testing and excavations

Subsequent to the magnetic study, we focused archaeological investigations on the two higher amplitude anomalies discussed above to evaluate the possible presence of archaeological features, such as building foundations, buried below the ground surface. Ultimately, we chose to investigate one with an excavation test unit. First we evaluated the area of both isolated anomalies with an in-depth surface reconnaissance.

The anomaly near ($x = 55$, $y = 5$) coincides with a linear surface feature which extends away from Cinnabar to the southeast. We interpret that linear feature to be a former field-access road or irrigation ditch, both of which are common to the project area

DOI: 10.1002/arp

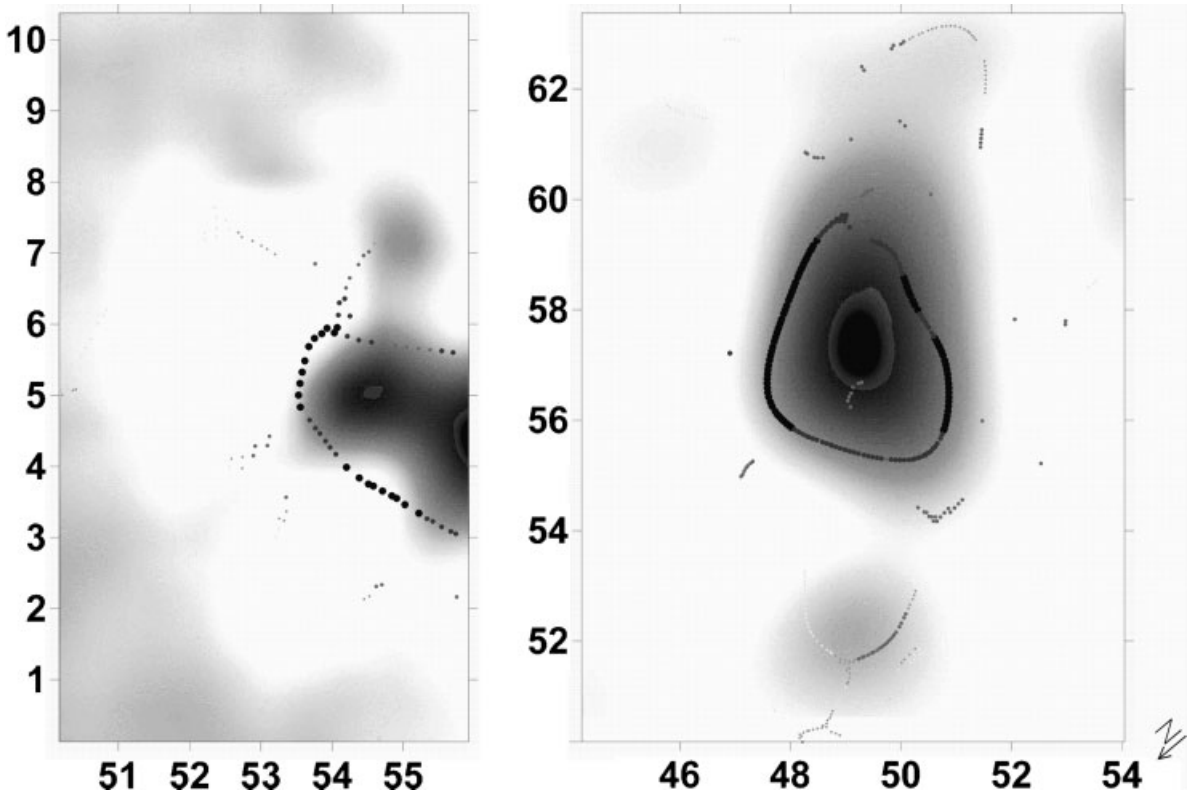

Figure 8. The grey-scale features are the plan view of the causative sources as determined by inverse modelling of the total field anomaly. The shaded dots are maxima of the horizontal gradient; darker and larger dots represent more significant maxima. In both cases, the larger maxima of the horizontal gradient of the field intensity coincide well with the edges of the causative sources as estimated independently by inversion.

due to the use of the area for agriculture in the early mid-twentieth century (prior to its purchase by Yellowstone National Park). Based on its association with the linear feature, we chose not to subject it to archaeological investigation thinking it has a lower potential for associated archaeological materials. However, based on our positive results from the second anomaly, there are probably remains of a buried historical structure along that old road or irrigation canal.

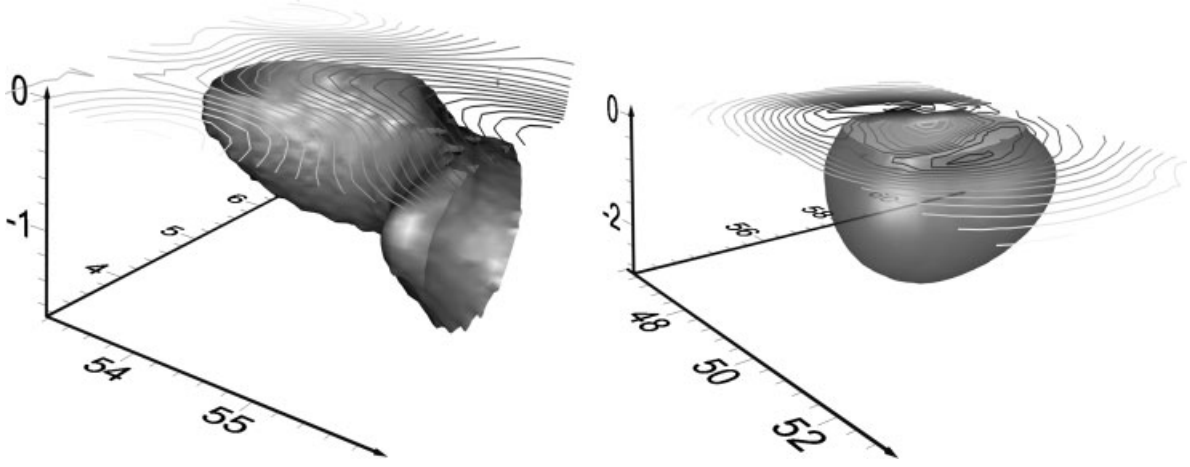

Figure 9. Three-dimensional renderings of solutions from the inverse modelling; contours are magnetic field intensity. The depicted isosurfaces are those near the maximum gradient of susceptibility in the inverse solutions.

DOI: 10.1002/arp

The area around the anomaly at ($x = 50$, $y = 57$) contained a scatter of historic glass and metal fragments on the ground surface, a possible indication of historic activity associated with Cinnabar. Thus, we excavated two 1 m^2 test units (TU) to investigate the strong magnetic signature of the area. TU 13 is within the central portion of the magnetic anomaly, while TU 14 is approximately 20 m to the west-northwest (Figure 2) outside the area of the larger anomalies (Figure 3). TU14 yielded limited artefacts including a few square nails, a cartridge, a button, and a suspender clip distributed within a few centimeters of the surface, perhaps indicating a house in the area.

Results of archaeological investigations in TU 13, within the magnetic anomaly, documented the presence of an intact archaeological feature within the area, probably associated with a former domestic structure on the southeastern flanks of Cinnabar. Of particular interest, TU 13 yielded a buried living floor containing burned wood fragments, charcoal, mortar, glass, and nails approximately 15–20 cm below ground surface (Figure 10). These artefacts indicate that a structure was present at one time, but possibly burned after or during the abandonment of Cinnabar in the early twentieth century. Excavation of TU 13 also identified plough scars stratigraphically above the building remains, suggesting that the area was ploughed in the early mid-twentieth century, further obscuring the presence of the former building. Finally, after agricultural use of the area ceased in the mid-1900s, a 10-cm-thick layer of silty aeolian sand blew over the surface of the feature, effectively masking its presence from the ground surface but not from magnetic detection.

Summary

One component of the Montana–Yellowstone Archaeological Project, a joint endeavour of The University of Montana Department of Anthropology and Yellowstone National Park, is determining the spatial extent of a historic town site, Cinnabar, Montana at the edge of Yellowstone National Park, USA. To help constrain

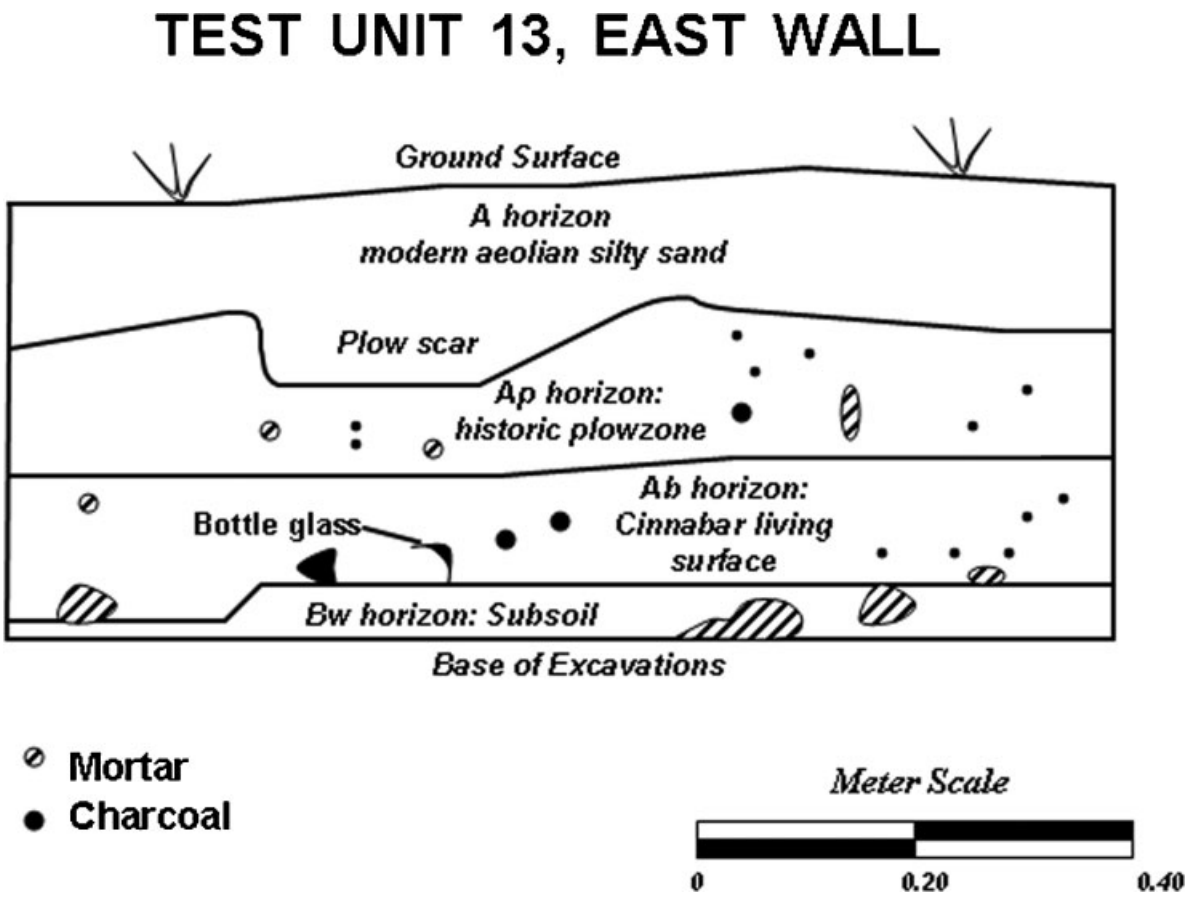

Figure 10. Profile of the east wall from a 1 m^2 excavation (Test Unit 13) on the south central anomaly at about $x = 50$ m, $y = 57$ m.

DOI: 10.1002/arp

the spatial extent of Cinnabar, we acquired total field magnetic intensity observations over a portion of the proposed southeast extent of the town. We then subjected those observations to filtering, edge detection, and modelling techniques common in aeromagnetic and ground magnetic exploration for energy and mineral resources.

We processed our data, which were originally quite noisy (Figure 3), by first subtracting a slightly dipping ambient field characterized by a first order, best-fit, polynomial surface. Next, we decorrugated the residual field with a two-dimensional frequency filter (Urquhart, 1988; Phillips, 2007), and then upward continued it (e.g. Blakely, 1995) by one half of the line spacing used during acquisition. These processing steps successfully isolated the longer wavelength anomalies characteristic of buried foundations or historic building perimeters and greatly reduced the dipolar noise from ferromagnetic objects distributed on the ground surface (Figure 6). Once we isolated the anomalies characteristic of foundations, we further accentuated them with standard edge detection and modelling techniques. The horizontal gradient method (HGM) of Blakely and Simpson (1986) provides good estimates of the edges of buried causative sources, which coincided well with edges determined by modelling (Figure 8). Nabighian et al. (2005) provide the history and complete referencing of these methods and we deem them successful in accentuating features of interest in areas where acquisition is difficult and/or surface scatter contributes significant high-frequency noise.

Test unit excavations within the south-central anomaly clearly indicate the remains of buried domestic features, perhaps the foundation to a house or other building associated with the late nineteenth to early twentieth century use of Cinnabar. The lack of surface indicators or adequate historic photography precluded the identification of this buried feature without the aid of the magnetic study. The result is that we identified an important and previously unidentified domestic feature of Cinnabar through the combined use of total field ground-acquired magnetic data, processing and filtering techniques common in the application of magnetics to energy and mineral exploration, and archaeological excavations. Unfortunately, TU13 was slightly mislocated and did not directly test the edge detection and modelling in that TU13 ended up inside the structure. Ultimately, the application of the two investigative approaches provided important historic archaeological data by which to interpret Cinnabar and its abandonment more than a century ago.

Acknowledgements

Gradient Geophysics Inc. of Missoula, Montana, distributor of MAG3D, provided use and support of MAG3D for our investigation of its use at the archaeological scale. We thank A. Johnson of Yellowstone National Park, and C. Whitacre of the Rocky Mountain Cooperative Ecosystem Unit for funding and logistical support for our archaeological endeavors. Two anonymous reviewers helped improve the manuscript.

References

Baranov V. 1957. A new method for interpretation of aeromagnetic maps pseudo-gravimetric anomalies. *Geophysics* **22**: 359–383.

Becker H. 2001. Duo- and quadro-sensor configuration for high-speed/high-resolution magnetic prospecting with cesium magnetometer. In *Magnetic Prospecting in Archaeological Sites*, Becker H, Fassbinder JWE (eds). International Council on Monuments and Sites: Munich; 20–25.

Blakely RJ. 1995. *Potential Theory in Gravity and Magnetic Applications*. Cambridge University Press: Cambridge.

Blakely RJ, Simpson RW. 1986. Approximating edges of source bodies from magnetic or gravity anomalies. *Geophysics* **51**: 1494–1498.

Ciminale M, Loddo M. 2001. Aspects of magnetic data processing. *Archaeological Prospection* **8**: 239–246.

Cooper GRJ, Cowan DR. 2008. Edge enhancement of potential-field data using normalized statistics. *Geophysics* **73**: H1–H4.

Fedi M, Florio GF. 2001. Detection of potential fields source boundaries by enhanced horizontal derivative method. *Geophysical Prospecting* **49**: 40–58.

Fedi M, Florio GF. 2003. Decorrugation and removal of directional trends of magnetic fields by the wavelet transform: application to archaeological areas. *Geophysical Prospecting* **51**: 261–272.

Gaffney C, Gaffney V, Cuttler R, Yorston R. 2008. Initial results using GPS navigation with the Foerster magnetometer system at the World Heritage Site of Cyrene, Libya. *Archaeological Prospection* **15**: 151–156.

Jacobsen B. 1987. A case for upward continuation as a standard separation filter for potential-field maps. *Geophysics* **52**: 1138–1148.

Kvamme KL. 1998. *Geophysical Explorations at the Wuamett Farmstead and the Huyser Farmstead, Minnesota Farmstead Study*. Unpublished report submitted to BRW, Inc.: Minneapolis, MN.

Larson TK, Domers LE, Penny DM, Hargrave ML. 1999. *Geophysical and Archaeological Investigations of Historic Sites at Fort Riley, Kansas*. Construction Engineering Research Laboratory Technical Report 99/47, US Army Corp of Engineers; 158 pp.

Li Y, Oldenburg DW. 1996. 3-D inversion of magnetic data. *Geophysics* **61**: 394–408.

MacDonald DH. 2007. *Final Inventory and Evaluation Report, Yellowstone National Park, Boundary Lands*

DOI: 10.1002/arp

Archaeological Survey & National Register Evaluation, Site 24YE355, Cinnabar/Yellowstone Bank Cache Site. Report submitted to Yellowstone National Park by The University of Montana Department of Anthropology: Missoula, MT.

MAG3D. 2007. A Program Library for Forward Modelling and Inversion of Magnetic Data over 3D Structures, version 4.0. Developed under the consortium research project *Joint/Cooperative Inversion of Geophysical and Geological Data*, UBC-Geophysical Inversion Facility, Department of Earth and Ocean Sciences, University of British Columbia: Vancouver, British Columbia.

Nabighian MN, Grauch VJS, Hansen RO, LaFehr TR, Li Y, Peirce JW, Phillips JD, Ruder ME. 2005. The historical development of the magnetic method in exploration. *Geophysics* **70**(6): 33–61.

NOAA. 2009. *United States National Oceanographic, Atmospheric Administration Space Weather Data and Products*. http://www.swpc.noaa.gov/Data/index.html; accessed 3/2009.

Odah H, Abdallatif TF, El-Hemaly IA, El-All EA. 2005. Gradiometer survey to locate the ancient remains distributed to the northeast of the Zoser Pyramid, Saqqara, Giza, Egypt. *Archaeological Prospection* **12**: 61–68.

Phillips JD. 1997. Potential-field geophysical software for the PC, version 2.2. *U.S. Geological Survey Open-File Report* **97–725**: 34 pp.

Phillips JD. 2007. Geosoft eXecutables (GX's) developed by the U.S. Geological Survey, version 2.0, with notes on GX development from Fortran code. *U.S. Geological Survey Open-File Report* **2007–1355**.

Phillips JD, Hansen RO, Blakely RJ. 2007. The use of curvature in potential-field interpretation. *Exploration Geophysics* **38**: 111–119.

Piro S, Sambuelli L, Godio A, Taormina R. 2007. Beyond image analysis in processing archaeomagnetic geophysical data: case studies of chamber tombs with dromos. *Near Surface Geophysics* **5**: 405–414.

Roest WR, Verhoef J, Pilkington M. 1992. Magnetic interpretation using the 3-D analytic signal. *Geophysics* **57**: 116–125.

Tabbagh J. 2003. Total field magnetic prospection: are vertical gradiometers measurements preferable to single sensor survey? *Archaeological Prospection* **10**: 75–81.

Thurston JB, Smith RS. 1997. Automatic conversion of magnetic data to depth, dip, and susceptibility contrast using the SPI method. *Geophysics* **62**: 807–813.

Tsivouraki B, Tsokas GN. 2007. Wavelet transform in denoising magnetic archaeological data. *Archaeological Prospection* **14**: 130–141.

Urquhart T. 1988. Decorrugation of enhanced magnetic field maps. *58th Annual International Meeting*, Society of Exploration Geophysicists, Expanded Abstracts; 371–372.

DOI: 10.1002/arp